UC Santa Barbara

Title

Radiosynthesis and in vivo evaluation of a novel σ 1 selective PET ligand

Permalink

https://escholarship.org/uc/item/1hd66903

Journal

RSC Medicinal Chemistry, 5(11)

ISSN

2040-2503

Authors

Jin, Hongjun
Fan, Jinda
Zhang, Xiang
et al.

Publication Date

2014-11-01

DOI

10.1039/c4md00240g

Peer reviewed

Radiosynthesis and *in vivo* evaluation of a novel σ₁ selective PET ligand

Hongjun Jin[a], **Jinda Fan**[a], **Xiang Zhang**[a], **Junfeng Li**[a], **Hubert P. Flores**[b], **Joel S. Perlmutter**[a,b], **Stanley M. Parsons**[c], and **Zhude Tu**[*,a]

[a]Department of Radiology, Washington University School of Medicine, St. Louis, MO, 63110, USA.

[b]Department of Neurology, Washington University School of Medicine, St. Louis, MO, 63110, USA.

[c]Department of Chemistry and Biochemistry, University of California, Santa Barbara, CA, 93106, USA.

Abstract

The σ_1 receptor is an important target for CNS disorders. We previously identified a σ_1 ligand TZ3108 having highly potent ($K_{i\text{-}\sigma1} = 0.48$ nM) and selective affinity for σ_1 versus σ_2 receptors. TZ3108 was ^{18}F-labeled with F-18 for *in vivo* evaluation. Biodistribution and blocking studies of [^{18}F]TZ3108 in male Sprague-Dawley rats demonstrated high brain uptake, which was σ_1-specific with no *in vivo* defluorination. MicroPET studies in cynomolgus macaques showed high brain penetration of [^{18}F]TZ3108; the regional brain distribution was consistent with that of the σ_1 receptor. Pseudo-equilibrium in the brain was reached ~ 45 min post-injection. Metabolite analysis of [^{18}F]TZ3108 in NHP blood and rodent blood and brain revealed that ~ 70% parent remained in the plasma of NHPs 60 min post-injection and the major radiometabolite did not cross the blood-brain barrier in rats. In summary, the potent, selective and metabolically stable σ_1 specific radioligand [^{18}F]TZ3108 represents a potentially useful PET radioligand for quantifying the σ_1 receptor in the brain.

Introduction

Sigma (σ) receptors were discovered in the 1970s and believed to be opioid receptors.[1–3] Subsequent pharmacological and structure activity studies determined that σ receptors are a distinct class of receptors with two subtypes, σ_1 and σ_2 receptors.[4] The σ_1 receptor is a molecular chaperone associated with neuroregulation and neuroprotection. The σ_1 receptor has been purified, sequenced and cloned; it is composed of 223 amino acids and is highly preserved across mammalian species. Its protein sequence does not share homology with any classic neurotransmitter or neuropeptide receptor.[5–7] The σ_2 receptor is overexpressed in

proliferating normal cells and tumors; although it has not been definitively identified, recent studies have proposed that progesterone receptor membrane component 1 is the σ_2 receptor binding site.[8, 9] The σ_1 receptor is highly expressed in the brain[10–12] and as well as several peripheral organs.[13] It is also associated with cancer cells and normal proliferating tissues.[5, 14] In knockout mice, a significant decrease in the hypermobility response has been measured.[15] In the central nervous system (CNS), the highest level of σ_1 transcription has been reported in various cranial nerve nuclei, followed by mesencephalic structures including substantia nigra, and in some diencephalic structures.[16, 17] On the basis of its broad modulatory effects, the σ_1 receptor is believed to play an important role in neuropsychiatric and neurodegenerative diseases. Recent studies of different σ_1 receptor agonists in animal models have shown positive therapeutic effects against CNS disorders including schizophrenia, depression[18–20] and in treating cocaine and methamphetamine addiction.[21–25]

Positron emission tomography (PET) is a noninvasive imaging modality that provides functional information about cellular processes. PET agents have been used for CNS imaging studies in preclinical animal models and used in human subjects.[26–35] [^{11}C]SA4503 is the only currently approved PET probe for imaging the σ_1 receptor. Although studies using [^{11}C]SA4503 have enhanced our understanding of the distribution of the σ_1 receptors in the CNS, considerable effort has been focused on developing metabolically stable ligands which bind reversibly to the receptor and reach equilibrium within 1–2 h post-injection. Although ^{18}F has a longer half-life than ^{11}C ($t_{1/2}$ = 109.8 min vs. 20.4 min) which places fewer time constraints on radiotracer synthesis or distribution and permits longer scan sessions that may increase target to non-target ratios, no ^{18}F-labeled PET probes have been approved yet for imaging the σ_1 receptor in human subjects. Most previously reported ^{18}F-labled tracers are limited by low affinity, low selectivity, low brain uptake, or have radiometabolites which could potentially confound modeling. Identifying an ^{18}F-labeled radiotracer with favorable in vivo pharmacokinetics would facilitate diagnostic and therapeutic applications for CNS disorders by permitting quantification of σ_1 receptor levels in the brain.

In studies of the well characterized piperidine heterocyclic amine pharmacophore, benzovesamicol analogues have shown high affinity for σ_1 receptor (Figure 1). We recently inserted a carbonyl group between the benzyl ring and the piperidine ring, substituted the proton with a fluorine atom, and introduced another aromatic ring at the other terminal.[36] This strategy identified a highly potent and selective σ_1 ligand, **TZ3108** ($K_{i\text{-}\sigma1}$ = 0.48 nM, $K_{i\text{-}\sigma2}$ = 1,740 nM, $K_{i\text{-}VAChT}$ = 1,360 nM, log P = 2.83).[36] The excellent *in vitro* selectivity of this racemic ligand for the σ_1 receptor suggested that ^{18}F-labeling might lead to the identification of a PET radiotracer for imaging the σ_1 receptor in the CNS. In this article, we report the radiosynthesis and the *in vivo* evaluation of [^{18}F]**TZ3108** in rats and nonhuman primates.

Results and Discussion

Chemistry and Radiochemistry

The nitro precursor **4** was synthesized according to the reported procedure with slight modifications (Scheme 1).[36, 37] From the commercially available 1,2,3,6-tetrahydropyridine, the epoxide compound **2** was obtained in two steps. Compound **3** was obtained by following our previously published procedure.[37–39] Coupling of **2** and **3** gave the racemic nitro precursor **4** in 71% yield.

The radiosynthesis of racemic [^{18}F]**TZ3108** was performed by a direct nucleophilic displacement of the nitro precursor, Compound **4**, using fluoride ([^{18}F]F$^-$). Aqueous [^{18}F]fluoride was azeotropically dried in presence of potassium carbonate as a base and Kryptofix 222 as a phase-transfer catalyst. Heating for 20 min at ~120 °C afforded [^{18}F]**TZ3108** in good radiochemical yield (RCY 18 – 24%, decay corrected). The reaction temperature was optimized to improve RCY. At temperatures below 120 °C, reaction kinetics were slow and resulted in lower yield; lower yields were also obtained at temperatures above 130 °C due to decomposition of nitro precursor **4**. The quantity of base used also had a significant impact on the RCY. Three equivalents of base were sufficient to accomplish the displacement reaction, while six equivalents of base resulted in significant decomposition of the precursor and corresponding low yield ($< 2\%$).

Rodent Biodistribution

The biodistribution of [^{18}F]**TZ3108** was evaluated in mature male Sprague-Dawley (SD) rats at 5, 30, and 60 min p.i. and uptake was calculated as %ID/g. Specific uptake was evaluated at 30 min p.i. following pre-treatment using two different blocking agents 5 min prior to tracer injection at 2 mg/kg: cold TZ3018, and the σ_1 receptor ligand Yun-122, *N*-(4-benzylcyclohexyl)-2-(2-fluorophenyl)acetamide were used. Yun-122 is a potent and selective σ_1 ligand (K_i-σ_1 = 3.6 nM, K_i-σ_2 = 667 nM) recently shown to be neuroprotective.[40, 41] The distribution of [^{18}F]**TZ3108** in peripheral organs and tissues is summarized in Table 1. Consistent with the distribution of the σ_1 receptor in peripheral tissues, lung showed the highest initial uptake for [^{18}F]**TZ3108** of 17.48 ± 4.38 (%ID/g) at 5 min p.i.; by 30 min activity in lung had reduced to 4.62 ± 1.16 % ID/g. Activity in blood was very low (0.07 %ID/g at 5 min p.i. and by 60 min p.i. had dropped to 0.03 %ID/g; activity in liver increased from 1.44 %ID/g at 5 min to 3.06 %ID/g by 60 min p.i., suggesting hepatobiliary clearance. No *in vivo* defluorination was observed: the bone uptake was 0.52 ± 0.12 %ID/g at 5 min and 0.58 ± 0.04 %ID/g at 60 min p.i.; the total bone uptake was low and the increase from 5 min to 60 min was negligible. As shown in Table 1, total brain showed strikingly high uptake and good retention. The uptake in total brain at 30 min was dramatically reduced by pre-treatment with 2 mg/kg of either cold **TZ3108** or Yun-122. In comparison with the no-carrier-added control group, total brain uptake (%I.D./g) in the pretreated group was reduced significantly from 1.32 to 0.98 when rats were pretreated using **TZ3108** and to 1.11 %ID/g when rats were pretreated using Yun-122 (p < 0.05). Uptake in peripheral tissues in blocking studies also showed reduced tracer levels in kidney, pancreas and heart. This is consistent with the σ_1 receptor distribution in these peripheral organs.[10–13] The increase observed in liver may reflect increased clearance when uptake in

target tissues is blocked. The regional brain distribution in rats is shown in Figure 2. [18F]**TZ3108** was evenly distributed among brain regions including brain stem, cortex, thalamus, striatum and hippocampus, while the uptake of [18F]**TZ3108** in cerebellum was 25–30% higher than the other regions. Uptake remained high in all brain regions at the 30 and 60 min time points. The observed distribution of [18F]**TZ3108** in both the brain and the peripheral organs of rats is consistent with the reported distribution of the σ_1 receptor.[10–13] Overall, these data suggest that [18F]**TZ3108** clears from the blood rapidly, shows specific uptake in σ_1 receptor enriched tissues, has no defluorination *in vivo*, and that [18F]**TZ3108** is able to penetrate the blood-brain barrier (BBB) to accumulate in regions of the brain known to express high levels of the σ_1 receptor.

MicroPET studies in NHPs

Based on the promising initial evaluation in rats, microPET imaging studies (n = 3) of [18F]**TZ3108** were performed in a male cynomolgus macaque using a microPET Focus 220 scanner. The summed images from 0 to 120 min were co-registered with MR images to accurately identify anatomical regions of interest within the brain. These microPET studies revealed high uptake of [18F]**TZ3108** in cerebellar and striatal regions and intermediate uptake in cortical regions, hippocampus and midbrain which all have high levels of the σ_1 receptor; modest uptake was seen in white matter. A representative set of imaging data and the corresponding time-activity curves (TAC) are shown in Figure 3. The NHP imaging studies indicate that [18F]**TZ3108** can readily cross the BBB and achieve pseudo-equilibrium binding; the distribution of [18F]**TZ3108** in NHP brain is consistent with the distribution of the σ_1 receptor.[10–12] The TACs (Figure 3B) indicate a steady-state accumulation of radioactivity in cerebellum and striatum within 30–45 min p.i., while significant accumulation of radioactivity in midbrain, frontal cortex, occipital cortex, temporal cortex and hippocampus was observed. Once steady-state was achieved, the standardized uptake values (SUV) remained relatively stable throughout the duration of the imaging session (120 min).

Metabolite analysis in NHPs and rats

Following tracer administration, radiometabolite analysis was performed on solvent extracts of plasma from NHP blood, rat blood and rat brain tissue to determine if [18F]**TZ3108** generates significant radioactive metabolites and if the radiometabolites could penetrate the BBB. Analysis of NHP blood samples showed that 65 – 75% of the radioactivity was in the plasma and 25 – 35% of the radioactivity was in packed red cells (PRC); 88 – 95% of the plasma-activity was in the supernatant and 5 – 12% was in the protein pellet. These results show that the supernatant contains the majority of the blood activity, suggesting that it represents the composition of the radioactivity in NHP plasma. Analysis of rat blood showed a similar distribution of activity; 70 – 76% of the activity from rat whole blood was in the plasma and 24 – 30% was in the PRC; the solvent extract contained 76% – 86% of the radioactivity while only 14 – 24% remained in the protein pellet. The solvent extraction process for rat brain homogenates yielded 62 – 66% in the supernatant and 34 – 38% in the tissue debris.

HPLC analysis of NHP plasma at 5, 15, 30 and 60 min as shown in Table 2 revealed only two radioactive peaks: a lipophilic metabolite (elution time 2–4 min) and the parent compound [^{18}F]**TZ3108** (elution time 9–12 min). At 5 min p.i., the solvent extract of plasma contained 97.9% parent compound; by 15 min p.i. HPLC analysis showed only 3.1% metabolite and 91.4% parent; by 30 min, the radiometabolite had only increased to 9.1% with >86% parent remaining; while at 60 min p.i, the HPLC analysis of NHP blood showed only ~21% radioactive metabolite with ~70% parent remaining.

Although analysis of radiometabolites in NHP blood during a typical PET imaging session demonstrated very promising stability 1 h post-injection, further HPLC metabolism studies were conducted in rats in order to determine if the observed radiometabolite was also found in rats and if it would cross the BBB. HPLC analysis of rat plasma samples identified three radioactive peaks at all-time points (Table 3). The first peak represented the major metabolite (Metabolite 1) and eluted at the same time as the radiometabolite seen in the NHP study. An additional minor peak (elution time 6–8 min) was identified in rats, and eluted immediately before the parent compound (9–12 min). The stability of [^{18}F]**TZ3108** in rats was similar to the results in NHPs; at 5 min p.i. 88.5% parent remained, by 30 min p.i., 86.5% parent was observed and at 60 min rat blood showed 78.2% parent; rat blood was also evaluated 90 min p.i. that showed 72% parent remaining. HPLC analysis of rat brain homogenate showed only trace levels (< 1%) of Metabolite 1 at every time point evaluated (Table 4). This suggests that Metabolite 1, which was the major radiometabolite found in both NHPs and rats, does not cross the BBB and would not impact PET data analysis for CNS imaging studies. More importantly, HPLC analysis demonstrated that [^{18}F]**TZ3108** is metabolically stable in both rodent and NHP blood. The dynamic microPET imaging showed clear tracer accumulation in the σ_1 receptor distribution regions, suggesting σ_1 receptor specific binding of [^{18}F]**TZ3108**.

Materials and methods

General

All analytical grade chemicals and reagents were purchased from Sigma-Aldrich (Milwaukee, WI) and were used without further purification unless otherwise specified. Flash column chromatography was conducted using silica gel, 60 Å, "40 Micron Flash" (32–63 μ), (Scientific Adsorbents, Inc., Atlanta, GA). Melting points were determined using MEL-TEMP 3.0 apparatus and uncorrected. 1H NMR spectra were recorded at 300 MHz on a Varian Mercury-VX spectrometer with CDCl$_3$ or DMSO-d$_6$ as solvent and tetramethylsilane (TMS) as the internal standard. All chemical shift values are reported in ppm (δ). Peak multiplicities were recorded as singlet, S; double, d; triplet, t, multiplet, m. Mass spectrometry was provided by the Washington University Mass Spectrometry Resource.

Chemistry

N-(4-Fluorobenzyl)-1,2,3,6-tetrahydropyridine (1)—To a reaction flask containing 1,2,3,6-tetrahydropyridine (0.5 g, 0.74 mmol) and triethylamine (1.82 g, 18 mmol) in CH$_2$Cl$_2$ (30 mL), 4-fluorobenzyl bromide (1.14 g, 0.74 mmol) was added dropwise. The

reaction mixture was stirred at room temperature (rt) overnight. Upon completion as determined by TLC, the mixture was washed with saturated Na_2CO_3 solution (30 mL) and brine (30 mL) sequentially. The organic phase was dried over Na_2SO_4 and concentrated under reduced pressure. The crude product was purified by chromatography (ethyl acetate: hexane, 1: 6) to afford compound **1** as colorless oil (0.81 g, 70 %). ^{1}H NMR (300 MHz, $CDCl_3$): δ 2.13–2.18 (m, 2 H, piperidine ring), 2.54 (t, $J = 5.6$ Hz, 2 H, piperidine ring), 2.93–2.97 (m, 2 H, piperidine ring), 3.54 (s, 2 H, CH_2), 5.63–5.38 (m, 2 H, CH=CH), 7.00–7.02 (m, 2 H, aromatic ring), 7.29–7.33 (m, 2 H, aromatic ring).

3-(4-Fluorobenzyl)-7-oxa-3-azabicyclo[4.1.0]heptane (2)—Compound **1** (2.20 g, 11.5 mmol) was added dropwise to a mixture of trifluoroacetic acid (1.31 g, 11.5 mmol) in water (20 mL), which was stirred at rt for 15 min. *N*-Bromosuccinimide (2.49 g, 14.0 mmol) was added in portions, and the reaction mixture was stirred at rt for 30 minutes. Another portion of *N*-bromosuccinimide (0.15 g 0.85 mmol) was added, the resulting mixture was stirred overnight at rt, then the supernatant was decanted. A 20% NaOH solution (20 mL) was added dropwise to the residue and stirred overnight at rt. The product was extracted with CH_2Cl_2 (50 mL × 3). The combined organic layers were sequentially washed with saturated Na_2CO_3 solution (100 mL) and brine (100 mL). The organic phase was dried over Na_2SO_4 and concentrated under reduced pressure. The crude product was purified by chromatography (ethyl acetate: hexane, 2: 3) to afford target product as colorless oil (1.93 g, 81%). ^{1}H NMR (300 MHz, $CDCl_3$): δ 1.89–2.04 (m, 2 H, piperidine ring), 2.13–2.31 (m, 2 H, piperidine ring), 2.64 (d, $J = 13.2$ Hz, 1 H, piperidine ring), 2.96 (dd, $J = 4.2, 13.5$ Hz, 1 H, piperidine ring), 3.16–3.19 (m, 2 H, piperidine ring), 3.39 (s, 2 H, CH_2), 6.94–7.03 (m, 2 H, aromatic ring), 7.22–7.27 (m, 2 H, aromatic ring).

(1′-(4-fluorobenzyl)-3′-hydroxy-[1,4′-bipiperidin]-4-yl)(4-nitrophenyl)methanone (4)—A mixture of compound **2** (0.36 g, 1.75 mmol), LiCl (73.6 mg, 1.75 mmol), and 4-(4-nitrobenzoyl)piperidine (**3**, 0.41 g, 1.75 mmol) in acetonitrile (ACN, 5 mL) was stirred at 40 °C overnight. The solvent was evaporated and the residue was dissolved in CH_2Cl_2 (20 mL). The CH_2Cl_2 was sequentially washed with saturated Na_2CO_3 solution (10 mL) and brine (10 mL). The organic phase was dried over Na_2SO_4 and concentrated under reduced pressure. The crude product was purified by chromatography (diethyl ether: Et_3N, 50:1) to afford **4** as the major product (yellow solid, 0.78 g, 71%, mp 116.2–118.5 °C). ^{1}H NMR (300 MHz, $CDCl_3$): δ 1.52–1.60 (m, 1 H, piperidine ring), 1.71–1.76 (m, 2 H, piperidine ring), 1.84–2.02 (m, 5 H, piperidine ring), 2.20–2.33 (m, 2 H, piperidine ring), 2.73–2.77 (m, 2 H, piperidine ring), 2.91–3.02 (m, 2 H, piperidine ring), 3.17–3.29 (m, 2 H, piperidine ring), 3.43 (s, 1 H, OH), 3.50 (s, 2 H, CH_2N), 3.59 (dt, $J = 4.8, 9.9$ Hz, 1 H, piperidine ring), 6.99 (d, $J = 8.7$ Hz, 2 H, aromatic ring), 7.25 (d, $J = 8.7$ Hz, 2 H, aromatic ring), 8.07 (d, $J = 8.7$ Hz, 2 H, aromatic ring), 8.32 (d, $J = 8.7$ Hz, 2 H, aromatic ring). HRMS (ESI) Calcd for $C_{24}H_{28}FN_3O_4$ (M+H)+ 442.2137, found: 442.2146.

Radiochemistry

Production of [18F]fluoride—[18F]Fluoride was produced by 18O(p, n)18F reaction through proton irradiation of enriched 18O water (95%) using Washington University's RDS111 cyclotron (Siemens/CTI Molecular Imaging, Knoxville, TN). [18F]Fluoride was

first passed through an ion-exchange resin and then eluted with 0.02 M potassium carbonate (K_2CO_3) solution.[37]

Radiosynthesis of [^{18}F] TZ3108—The ^{18}F-labeling of [^{18}F]**TZ3108** is outlined in Scheme 2. A sample of ~5.55 Gbq [^{18}F]fluoride/K_2CO_3 (~0.5 mg) was added to a reaction vessel containing Kryptofix 222 (5–6 mg) and dried by azeotropic distillation at 110 °C using ACN (3×1 mL) under a gentle flow of N_2 gas. After all water was removed, 1.5 – 2.0 mg of the nitro precursor, **4**, dissolved in DMSO (200 μL) was transferred to the reaction vessel containing [^{18}F]fluoride/ Kryptofix 222/K_2CO_3. The reaction vessel was capped, briefly mixed, and heated in an oil bath at 120 °C for 15–20 min. The reaction was monitored by TLC using methanol: methylene chloride (25: 75). The R_f value of the product is approximately 0.90. After removing the heat source, the reaction mixture was diluted with 3.0 mL of HPLC mobile phase (see below) and passed through an alumina Neutral Sep-Pak Plus cartridge. The crude product was purified using a semi-preparative HPLC system which contains a 5-mL injection loop, a Phenomenex Luna C-18 semi-preparative column (250 mm × 9.4 mm), UV detector at 254 nm, and an in-line radioactivity detector. Using a mobile phase of acetonitrile: 0.1 M ammonium formate buffer, pH 4.5 (21: 79) at 4.0 mL/min, the retention time of **TZ3108** was 29.2 min; the retention time of the precursor **4** was 32.3 min. The desired product was collected in a vial containing 50 mL sterile water, then the diluted eluent was trapped on a C-18 Plus Sep-Pak cartridge, which was rinsed with 10 mL sterile water, The final product was eluted with 0.6 mL ethanol followed by 5.4 mL saline. The diluted [^{18}F]**TZ3108** was passed through a 0.22 μm syringe filter into a sterile glass vial, and an aliquot was removed for QC testing. The radioactive dose was authenticated by co-injection with the corresponding cold reference compound **TZ3108** using an analytical HPLC system that consisted of a Phenomenex Prodigy C-18 analytical column (250 mm × 4.6 mm), and a UV detector at 254 nm. Using a mobile phase of acetonitrile: 0.1 M ammonium formate buffer, pH 4.5 (38: 62), with a flow rate of 1.0 mL/min, the retention time of [^{18}F]**TZ3108** was 4.7 min; the retention time of precursor **4** was 5.1 min. Radiochemical purity was > 99%, chemical purity was > 95%, RCY was 18 – 24% (n > 10, decay-corrected) and the specific activity was > 74 GBq/μmol (decay-corrected to end of synthesis). The total synthesis time was ~ 2 h.

In vivo biodistribution and regional brain uptake in rats

All animal experiments were conducted in compliance with the Guidelines for the Care and Use of Research Animals under protocols approved by the Washington University Animal Studies Committee. For the biodistribution studies, ~2.5 Mbq of [^{18}F]**TZ3108** was injected in the tail vein of 200–350 g mature male SD rats under anesthesia (2.5% isoflurane in oxygen). Blocking was evaluated at 30 min post-injection (p.i.) using 2 mg/kg of either cold **TZ3108** or Yun-122 injected 5 min prior to the tracer. At 5, 30, and 60 min p.i., the rats (n = 4 per study group) were euthanized under anesthesia. The whole brain was quickly removed and the hippocampus, striatum, cortex, thalamus, brain stem, and cerebellum were separated by gross dissection. The remainder of the brain was collected to determine total brain uptake. Peripheral tissues including blood, heart, lung, liver, spleen, pancreas, kidney, muscle, fat and bone were also collected. Samples were weighed and counted in an

automated gamma counter using diluted injectate as a standard, and the percent injected dose per gram (%ID/g) was calculated.

In vivo microPET brain imaging studies in male monkey

Three independent PET studies of [^{18}F]**TZ3108** were performed on an adult male cynomolgus macaque (~ 4 – 6 kg) using a microPET Focus 220 scanner (Concorde/CTI/ Siemens Microsystems, Knoxville, TN). MicroPET imaging was performed as previously described.[37, 42] The monkey was initially anesthetized using an intramuscular injection of ketamine and glycopyrulate. It was then transported to the PET scanner suite, and intubated, and percutaneous catheters were placed for venous tracer injection and arterial blood sampling. The head was positioned supine in the adjustable head holder with the brain in the center of the field of view (FOV). Anesthesia was maintained at 1.5 – 2.0% isoflurane in oxygen and core temperature maintained at ~37 °C. A 10 min transmission scan was performed to confirm position of the target regions within the FOV; this was followed by a 45 min transmission scan for attenuation correction. Subsequently, a 120 min dynamic emission scan was acquired (3 × 1 min, 4 × 2 min, 3 × 3-min, and 20 × 5 min frames) after injection of 240–360 MBq [^{18}F]**TZ3108**.

MicroPET image data processing and analysis

PET scans were corrected using individual attenuation and model-based scatter correction and reconstructed using filtered back projection as described previously.[43] Prior to PET data analysis, PET images were aligned with other PET images from that same study session using automated image registration program AIR.[44, 45] The resolution of the reconstructed PET image at the center of the FOV was < 2.0 mm full width half maximum for all three dimensions. The MPRAGE-MRI anatomical scan was co-registered to the PET scan of the same subject using AIR method, and the traced volumes of interest (VOIs) were transformed into PET space using the same transformation matrix.[46] For quantitative analyses, three-dimensional regions of interest (ROI) including cerebellum, frontal occipital, striatum, temporal, white matter, midbrain and hippocampus were then overlaid on all reconstructed PET images to obtain tissue time–activity curves (TACs). Activity measures were standardized to body weight and dose of radioactivity injected to yield standardized uptake value (SUV).

HPLC Metabolite analysis

To determine if radiometabolites of [^{18}F]**TZ3108** would cross the BBB in a nonhuman primate, HPLC analysis was performed for samples including NHP arterial blood plasma, rat plasma, and homogenized rat brain tissue after injection of [^{18}F]**TZ3108**. The percentage of parent compound versus the percentage of radiolabeled metabolites was determined for each sample. The HPLC system consisted of an Agilent SB C-18 analytical HPLC column (250 mm × 4.6 mm, 5 μA) with a 200 μL injection loop and an UV detector with wavelength set at 254 nm. The mobile phase was acetonitrile: 0.1 M ammonium formate buffer, pH 4.5 (32: 68). Fractions were collected at 1 min intervals for 16 min, counted in a well counter and then background and decay-corrected. At a flow rate of 1.0 mL/min the parent

compound [^{18}F]**TZ3108** eluted at ~10.5 min. A reserved aliquot of the tracer was processed in the same manner as the biological samples to confirm the identity of the parent peak.

Metabolite analysis of NHP arterial blood plasma—Arterial blood samples (~1.5 mL) were collected during a microPET imaging session at 5, 15, 30 and 60 min p.i. from a percutaneous catheter in a heparinized syringe. 1 mL aliquots were counted in a well counter and then centrifuged to separate red blood cells from plasma. Aliquots of plasma (400 μL) were deproteinated with 0.93 mL of ice-cold methanol; the protein pellet was separated from the solvent extract by centrifugation at 4 °C for 5 min (15,000 × g). A 200 μL aliquot of the supernatant was mixed with water (1:1) and injected onto the HPLC system for metabolite analysis as described above.

Metabolite analysis of rat brain and rat plasma—Adult male SD rats were injected with [^{18}F]**TZ3108** under anesthesia and euthanized for tissue collection as previously described for the biodistribution studies. Because the tracer rapidly clears the blood in rats (see Table 1), in order to ensure the blood and brain extracts would have adequate counts for HPLC analysis, rats were injected with 41 MBq for the 5 min time point, 76 MBq for 30 min, 88.8 MBq for 60 min and 125.8 MBq for determination of radiometabolites 90 min p.i. Rats were euthanized under anesthesia and heparinized whole blood samples were collected and processed as described above for NHP blood samples. The whole brain was rapidly removed, blotted to remove blood, and homogenized on ice with 0.5 mL of saline. The whole brain homogenate was extracted with 1.2 mL ice-cold methanol. A 1.0 mL aliquot of the brain homogenate and solvent mixture was centrifuged at 4 °C for 5 min (15,000 × g) to pellet tissue debris; the supernatant was diluted with water 1:1 for HPLC analysis as described above.

Conclusions

TZ3108 was previously identified by our group as a highly potent and highly selective σ$_1$ receptor ligand.[36] Here we report the successful radiosynthesis of racemic [^{18}F]**TZ3108** in high yield. Biodistribution studies in rats and microPET imaging studies in cynomolgus macaque demonstrated that [^{18}F]**TZ3108** has high brain uptake in both rats and NHPs. Pretreatment of the rats with both cold **TZ3108** and the σ$_1$ specific compound Yun-122 significantly reduced the uptake in target tissues, suggesting that brain uptake is specific. MicroPET imaging studies in NHPs showed excellent visualization of anatomical structures; SUV analysis yielded TACs with steady-state levels by 45 min p.i. Metabolite analysis of NHP plasma solvent extracts showed ~70% intact parent compound at 60 min p.i.; rodent blood and brain HPLC metabolism studies showed that the radiometabolite observed in NHPs does not cross the rat BBB. Although the data we report here collectively suggest that **TZ3108** may yield a PET probe to image σ$_1$ receptors in the brain, it is well known that σ$_1$ receptor binding has stereo-selectivity.[47–49] The promising results from the racemic compound [^{18}F]**TZ3108** inspires further investigation of the resolved [^{18}F]**TZ3108** isomers Once the racemic compound **TZ3108** is resolved and the enantiomers radiolabeled for further studies, one enantiomer may have the metabolic stability and pharmacodynamics needed for a clinical PET tracer for the σ$_1$ receptor.

Supplementary Material

Refer to Web version on PubMed Central for supplementary material.

Acknowledgements

Abbreviations

|	
ACN	acetonitrile
AD	Alzheimer's disease
AIR	automated image registration
CNS	central nervous system
DMSO	Dimethyl sulfoxide
BBB	blood–brain barrier
Bq	becquerel
ESI	electrospray ionization
FOV	field of view
HRMS	high-resolution mass spectrometry
Kryptofix 222	commercially available cryptand sold under the tradename Kryptofix (4,7,13,16,21,24-Hexaoxa-1,10-diazabicyclo[8.8.8]hexacosane (CAS: 23978-09-8), particularly with high affinity for alkali metal cations, which has allowed the isolation of salts of K^+
MPRAGE	magnetization-prepared rapid acquisition gradient
MRI	magnetic resonance imaging
MEL-TEMP	melting point apparatus
NHP	non-human primate
p.i.	post-injection
%ID/g	percentile injection dose per gram
PET	positron emission tomography
PRC	packed red cells
QC	quality control
RCY	radiochemical yield
ROI	regions of interest
Yun-122	N-(4-benzylcyclohexyl)-2-(2-fluorophenyl)acetamide

rt	room temperature
SD	Sprague-Dawley
SUV	standard uptake value
TAC	time-activity curve
TLC	Thin-layer chromatography
TMS	tetramethylsilane
VOI	volumes of interest

References

1. Gilbert PE, Martin WR. Drug Alcohol Depend. 1976; 1:373–376. [PubMed: 189982]

2. Gilbert PE, Martin WR. J Pharmacol Exp Ther. 1976; 198:66–82. [PubMed: 945350]

3. Martin WR, Eades CG, Thompson JA, Huppler RE, Gilbert PE. J Pharmacol Exp Ther. 1976; 197:517–532. [PubMed: 945347]

4. Walker JM, Bowen WD, Walker FO, Matsumoto RR, De Costa B, Rice KC. Pharmacol Rev. 1990; 42:355–402. [PubMed: 1964225]

5. Maurice T, Su T-P. Pharmacol Ther. 2009; 124:195–206. [PubMed: 19619582]

6. Hanner M, Moebius FF, Flandorfer A, Knaus HG, Striessnig J, Kempner E, Glossmann H. Proc Natl Acad Sci U S A. 1996; 93:8072–8077. [PubMed: 8755605]

7. Kekuda R, Prasad PD, Fei YJ, Leibach FH, Ganapathy V. Biochem Biophys Res Commun. 1996; 229:553–558. [PubMed: 8954936]

8. Hornick JR, Spitzer D, Goedegebuure P, Mach RH, Hawkins WG. Surgery. 2012; 152:S152–S156. [PubMed: 22763259]

9. Xu J, Zeng C, Chu W, Pan F, Rothfuss JM, Zhang F, Tu Z, Zhou D, Zeng D, Vangveravong S, Johnston F, Spitzer D, Chang KC, Hotchkiss RS, Hawkins WG, Wheeler KT, Mach RH. Nat Commun. 2011; 2:380. [PubMed: 21730960]

10. Sakata M, Kimura Y, Naganawa M, Oda K, Ishii K, Chihara K, Ishiwata K. Neuroimage. 2007; 35:1–8. [PubMed: 17240168]

11. Mash DC, Zabetian CP. Synapse. 1992; 12:195–205. [PubMed: 1481139]

12. Weissman AD, Su TP, Hedreen JC, London ED. J Pharmacol Exp Ther. 1988; 247:29–33. [PubMed: 2845055]

13. Maestrup EG, Fischer S, Wiese C, Schepmann D, Hiller A, Deuther-Conrad W, Steinbach J, Wunsch B, Brust P. J Med Chem. 2009; 52:6062–6072. [PubMed: 19791807]

14. van Waarde A, Rybczynska AA, Ramakrishnan N, Ishiwata K, Elsinga PH, Dierckx RA. Curr Pharm Des. 2010; 16:3519–3537. [PubMed: 21050178]

15. Langa F, Codony X, Tovar V, Lavado A, Gimenez E, Cozar P, Cantero M, Dordal A, Hernandez E, Perez R, Monroy X, Zamanillo D, Guitart X, Montoliu L. Eur J Neurosci. 2003; 18:2188–2196. [PubMed: 14622179]

16. Vidal H, Mondesert G, Galiegue S, Carriere D, Dupuy P-H, Carayon P, Combes T, Bribes E, Simony-Lafontaine J, Kramar A, Loison G, Casellas P. Cancer Res. 2003; 63:4809–4818. [PubMed: 12941800]

17. Kitaichi K, Chabot JG, Moebius FF, Flandorfer A, Glossmann H, Quirion R. J Chem Neuroanat. 2000; 20:375–387. [PubMed: 11207432]

18. Hedskog L, Pinho CM, Filadi R, Ronnback A, Hertwig L, Wiehager B, Larssen P, Gellhaar S, Sandebring A, Westerlund M, Graff C, Winblad B, Galter D, Behbahani H, Pizzo P, Glaser E, Ankarcrona M. Proc Natl Acad Sci U S A. 2013; 110:7916–7921. [PubMed: 23620518]

19. Feher A, Juhasz A, Laszlo A, Kalman J Jr. Pakaski M, Kalman J, Janka Z. Neurosci Lett. 2012; 517:136–139. [PubMed: 22561649]

20. Villard V, Meunier J, Chevallier N, Maurice T. J Pharmacol Sci. 2011; 115:279–292. [PubMed: 21427517]

21. Yao H, Kim K, Duan M, Hayashi T, Guo M, Morgello S, Prat A, Wang J, Su T-P, Buch S. J Neurosci. 2011; 31:5942–5955. [PubMed: 21508219]

22. Ramachandran S, Chu UB, Mavlyutov TA, Pal A, Pyne S, Ruoho AE. Eur J Pharmacol. 2009; 609:19–26. [PubMed: 19285059]

23. Xu Y-T, Robson MJ, Szeszel-Fedorowicz W, Patel D, Rooney R, McCurdy CR, Matsumoto RR. Pharmacol Biochem Behav. 2012; 101:174–180. [PubMed: 22234290]

24. Seminerio MJ, Hansen R, Kaushal N, Zhang HT, McCurdy CR, Matsumoto RR. Int J Neuropsychopharmacol. 2013; 16:1033–1044. [PubMed: 22932447]

25. Robson MJ, Noorbakhsh B, Seminerio MJ, Matsumoto RR. Curr Pharm Des. 2012; 18:902–919. [PubMed: 22288407]

26. Toyohara J, Sakata M, Ishiwata K. Cent Nerv Syst Agents Med Chem. 2009; 9:190–196. [PubMed: 20021353]

27. Ishikawa M, Sakata M, Ishii K, Kimura Y, Oda K, Toyohara J, Wu J, Ishiwata K, Iyo M, Hashimoto K. Int J Neuropsychopharmacol. 2009; 12:1127–1131. [PubMed: 19573265]

28. Ishikawa M, Ishiwata K, Ishii K, Kimura Y, Sakata M, Naganawa M, Oda K, Miyatake R, Fujisaki M, Shimizu E, Shirayama Y, Iyo M, Hashimoto K. Biol Psychiatry. 2007; 62:878–883. [PubMed: 17662961]

29. Ishiwata K, Kawamura K, Yajima K, QingGeLeTu, Mori H, Shiba K. Nucl Med Biol. 2006; 33:543–548. [PubMed: 16720247]

30. Elsinga PH, Tsukada H, Harada N, Kakiuchi T, Kawamura K, Vaalburg W, Kimura Y, Kobayashi T, Ishiwata K. Synapse. 2004; 52:29–37. [PubMed: 14755630]

31. Kawamura K, Ishiwata K, Tajima H, Ishii S, Matsuno K, Homma Y, Senda M. Nucl Med Biol. 2000; 27:255–261. [PubMed: 10832082]

32. Kortekaas R, Maguire RP, van Waarde A, Leenders KL, Elsinga PH. Neurochem Int. 2008; 53:45–50. [PubMed: 18571772]

33. Brust P, Deuther-Conrad W, Lehmkuhl K, Jia H, Wunsch B. Curr Med Chem. 2014; 21:35–69. [PubMed: 23992342]

34. Fischer S, Wiese C, Maestrup EG, Hiller A, Deuther-Conrad W, Scheunemann M, Schepmann D, Steinbach J, Wunsch B, Brust P. Eur J Nucl Med Mol Imaging. 2011; 38:540–551. [PubMed: 21072511]

35. Waterhouse RN, Chang RC, Zhao J, Carambot PE. Nucl Med Biol. 2006; 33:211–215. [PubMed: 16546675]

36. Wang W, Cui J, Lu X, Padakanti PK, Xu J, Parsons SM, Luedtke RR, Rath NP, Tu Z. J Med Chem. 2011; 54:5362–5372. [PubMed: 21732626]

37. Tu Z, Efange SM, Xu J, Li S, Jones LA, Parsons SM, Mach RH. J Med Chem. 2009; 52:1358–1369. [PubMed: 19203271]

38. Li J, Zhang X, Zhang Z, Padakanti PK, Jin H, Cui J, Li A, Zeng D, Rath NP, Flores H, Perlmutter JS, Parsons SM, Tu Z. J Med Chem. 2013; 56:6216–6233. [PubMed: 23802889]

39. Efange SM, Khare AB, von Hohenberg K, Mach RH, Parsons SM, Tu Z. J Med Chem. 2010; 53:2825–2835. [PubMed: 20218624]

40. Huang Y, Hammond PS, Whirrett BR, Kuhner RJ, Wu L, Childers SR, Mach RH. J Med Chem. 1998; 41:2361–2370. [PubMed: 9632369]

41. Luedtke RR, Perez E, Yang SH, Liu R, Vangveravong S, Tu Z, Mach RH, Simpkins JW. Brain Res. 2012; 1441:17–26. [PubMed: 22285434]

42. Fan J, Zhang X, Li J, Jin H, Padakanti PK, Jones LA, Flores HP, Su Y, Perlmutter JS, Tu Z. Bioorg Med Chem. 2014; 22:2648–2654. [PubMed: 24721831]

43. Criswell SR, Perlmutter JS, Videen TO, Moerlein SM, Flores HP, Birke AM, Racette BA. Neurology. 2011; 76:1296–1301. [PubMed: 21471467]

44. Tabbal SD, Mink JW, Antenor JA, Carl JL, Moerlein SM, Perlmutter JS. Neuroscience. 2006; 141:1281–1287. [PubMed: 16766129]

45. Woods RP, Mazziotta JC, Cherry SR. J Comput Assist Tomogr. 1993; 17:536–546. [PubMed: 8331222]

46. Karimi M, Tian L, Brown CA, Flores HP, Loftin SK, Videen TO, Moerlein SM, Perlmutter JS. Ann Neurol. 2013; 73:390–396. [PubMed: 23423933]

47. Georg A, Friedl A. J Pharmacol Exp Ther. 1991; 259:479–483. [PubMed: 1658298]

48. Hellewell SB, Bowen WD. Brain Res. 1990; 527:244–253. [PubMed: 2174717]

49. Hayashi T, Su TP. Expert Opin Ther Targets. 2008; 12:45–58. [PubMed: 18076369]
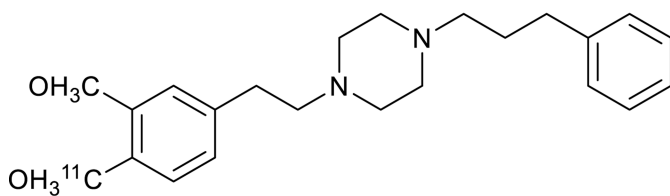
[^{11}C]**SA4503**
$K_{i-\sigma1}$ = 4.4 nM
$K_{i-\sigma2}$ = 242 nM
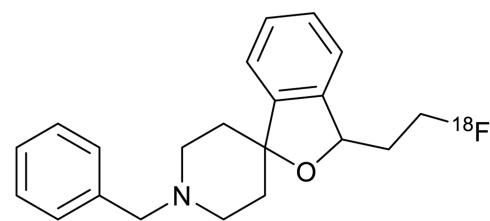
[^{18}F]Fluspidine
$K_{i-\sigma1}$ = 0.59 nM
$K_{i-\sigma2}$ = 708 nM
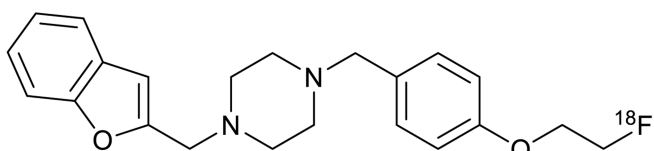
[^{18}F]piperazine derivative
$K_{i-\sigma1}$ = 2.6 nM
$K_{i-\sigma2}$ = 486 nM
$K_{i-5-HT2B}$ = 96 nM
K_{i-D2} > 10,000 nM
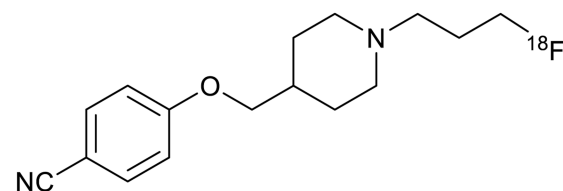
[^{18}F]**2-FPS**
$K_{i-\sigma1}$ = 4.3 nM
$K_{i-\sigma2}$ = 143 nM
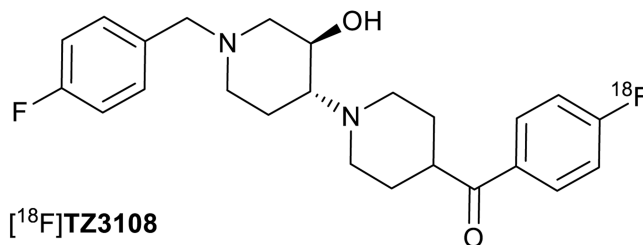
[^{18}F]**TZ3108**
$K_{i-\sigma1}$ = 0.48 ± 0.14 nM
$K_{i-\sigma2}$ = 1740 ± 280 nM
σ_1/σ_2 = 3,600-fold
$K_{i-VAChT}$ = 1,360 ± 295 nM
K_{i-D2} = 1,350 ± 53 nM
K_{i-D3} > 20,000 nM

Figure 1.
The structure and binding affinity of [^{18}F]**TZ3108** and other reported σ_1-selective PET tracers
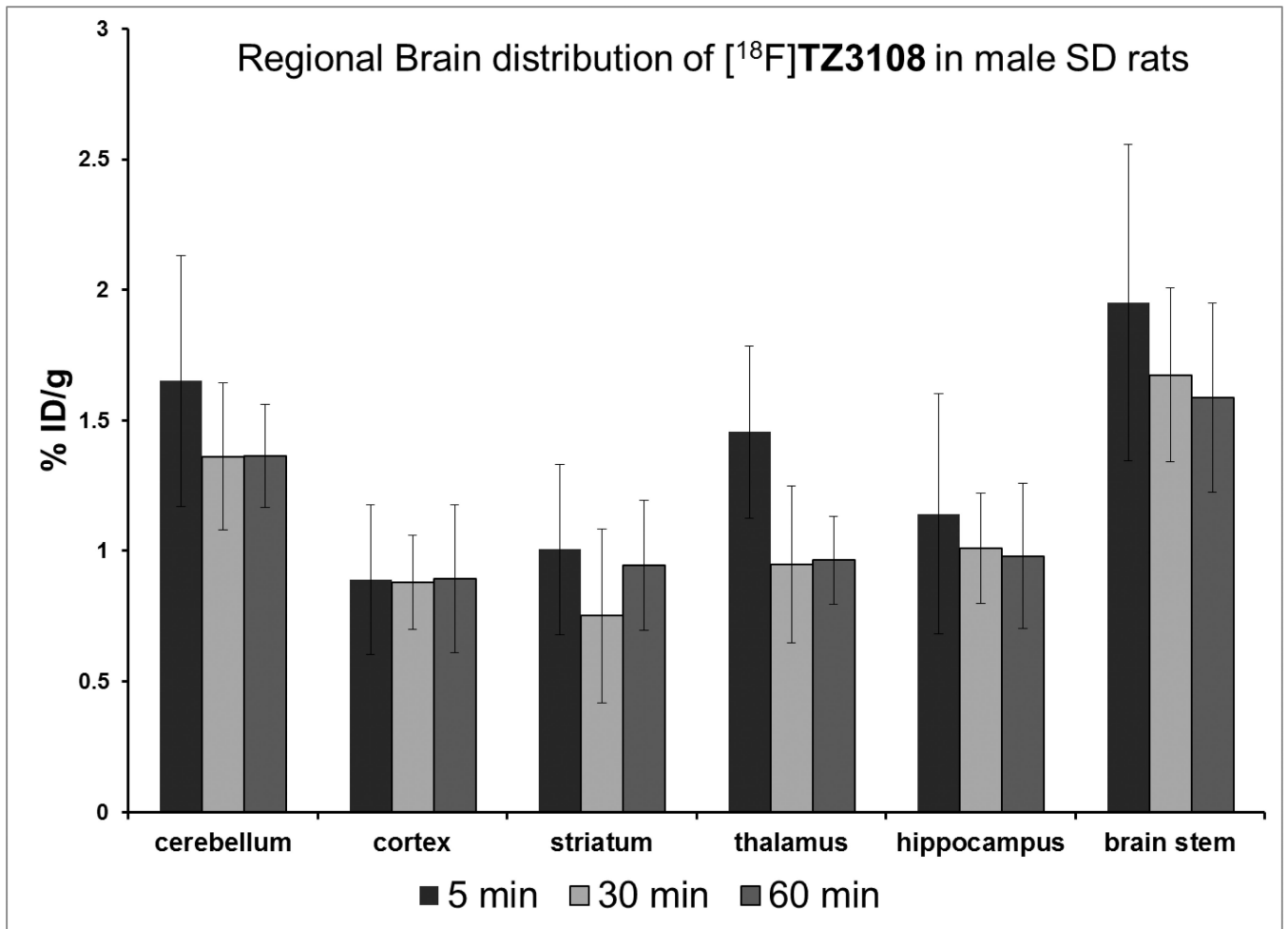
Figure 2.
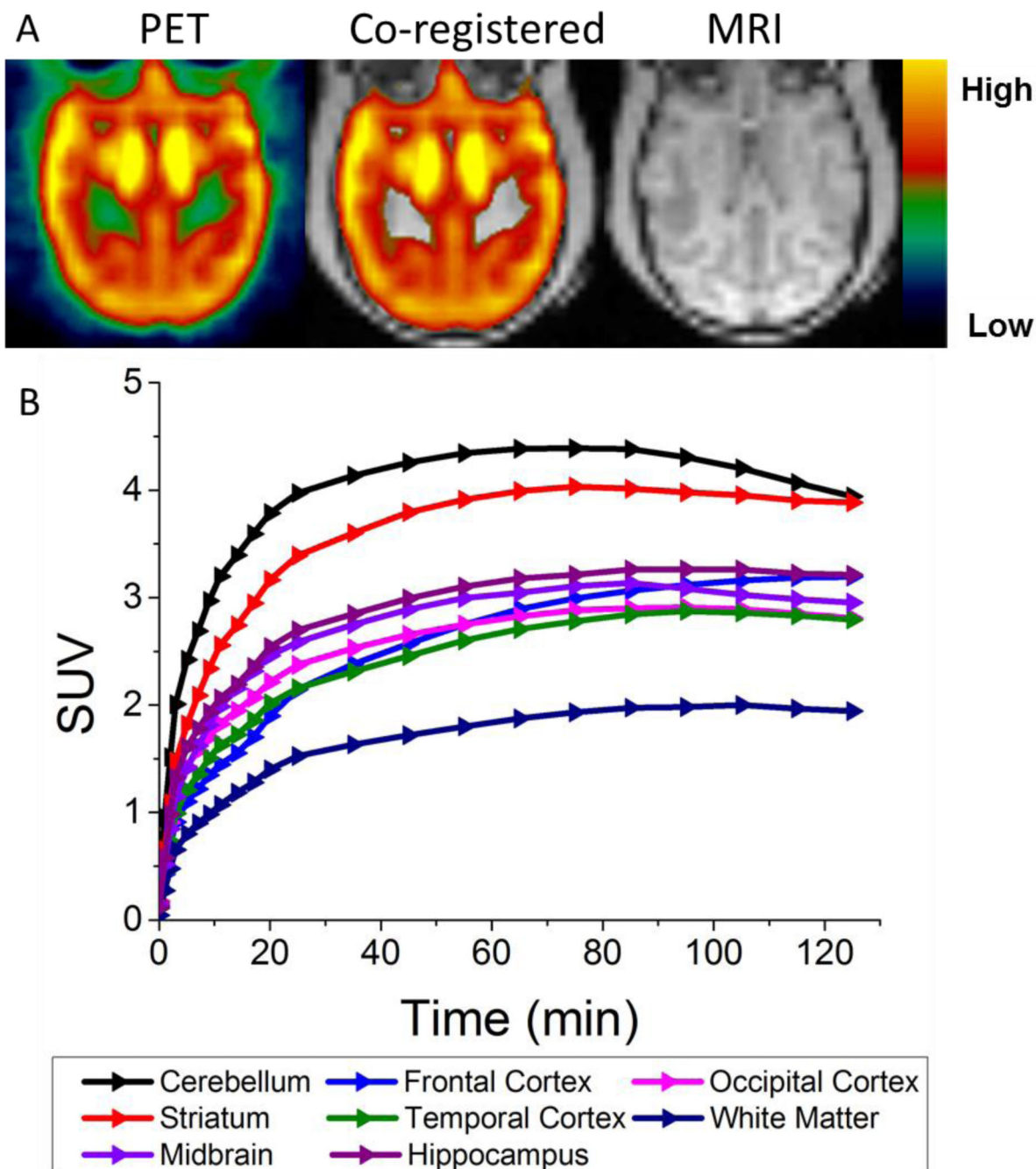Regional brain distribution in male SD rats

Figure 3.
CNS microPET imaging of [^{18}F]**TZ3108** in a male cynomolgus macaque
A: Representative image (summed) **Left**: PET image; **middle**: Co-registration of MRI and PET, **right**: MR image.
**B**: Corresponding time activity curve (TAC). Highest uptake was seen in cerebellum and striatum, lower uptake was seen in white matter, with intermediate uptake in cortical regions, midbrain and hippocampus.
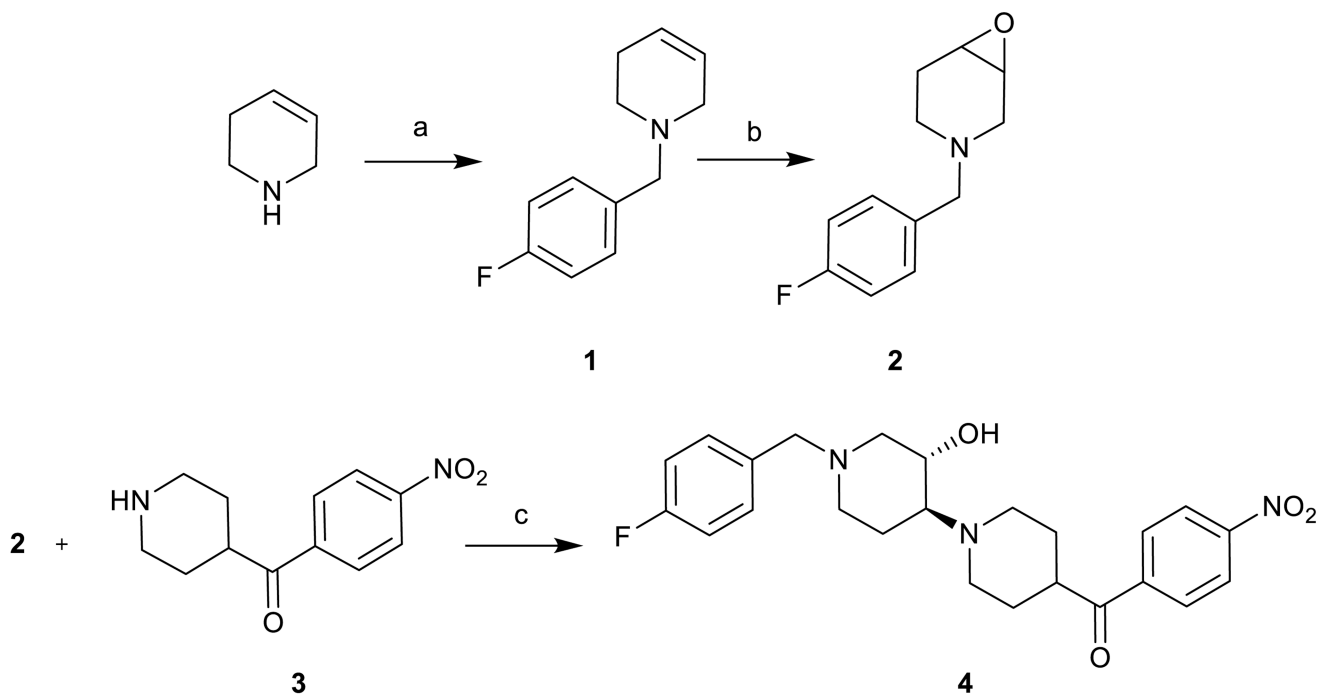
Reagents and conditions:

(a) 4-fluorobenzyl chloride, Et$_3$N, CH$_2$Cl$_2$, rt, overnight, 70%; (b) i) TFA, NBS, H$_2$O, rt, overnight; ii) NaOH, rt, overnight, 81%; (c) LiCl, ACN, 40 °C, overnight, 71%,

Scheme 1.
Synthesis of precursor (Compound **4**)
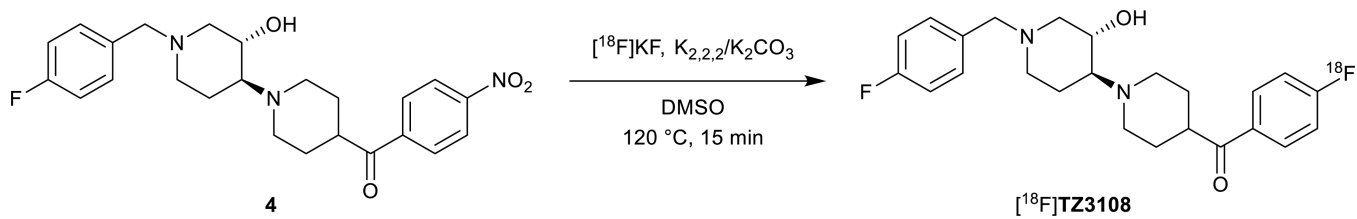
Scheme 2.
Radiosynthesis of [^{18}F]**TZ3108**

Table 1

Biodistribution of [^{18}F]**TZ3108** in male SD rats (mean ± SD, n = 4)

	5 min	30 min	30 min.TZ3108	30 min.Yun-122	60 min
blood	0.074 ± 0.021	0.028 ± 0.004	0.049 ± 0.008	0.034 ± 0.002	0.025 ± 0.004
lung	17.48 ± 4.38	4.621 ± 1.159	4.904 ± 0.592	3.944 ± 1.030	3.521 ± 0.464
liver	1.436 ± 0.510	1.838 ± 1.225	3.196 ± 0.495	3.231 ± 0.539	3.060 ± 0.653
spleen	3.064 ± 1.189	2.466 ± 0.518	2.391 ± 0.837	3.265 ± 0.665	1.635 ± 0.840
kidney	3.523 ± 0.530	3.089 ± 0.718	1.724 ± 0.191 *	2.261 ± 0.303 *	2.675 ± 1.115
pancreas	1.312 ± 0.226	1.449 ± 0.291	0.713 ± 0.268 *	0.786 ± 0.045 *	1.567 ± 0.140
muscle	0.146 ± 0.019	0.094 ± 0.048	0.143 ± 0.080	0.147 ± 0.005	0.074 ± 0.021
Fat	0.181 ± 0.073	0.167 ± 0.028	0.202 ± 0.023	0.162 ± 0.029	0.136 ± 0.084
heart	1.603 ± 0.218	0.637 ± 0.105	0.488 ± 0.061	0.390 ± 0.061 *	0.533 ± 0.067
bone	0.516 ± 0.121	0.507 ± 0.040	0.550 ± 0.069	0.572 ± 0.078	0.577 ± 0.040
total brain	1.586 ± 0.505	1.324 ± 0.127	0.977 ± 0.137 *	1.110 ± 0.131 *	1.321 ± 0.082

*
Student t test showed significant decrease (p<0.05) between blocking and no carrier added groups.

Table 2

HPLC metabolite analysis of NHP blood

	5 min	15 min	30 min	60 min
[^{18}F]**TZ3108**	97.7%	91.4%	86.5%	69.4%
Metabolite 1	0.77%	3.3%	9.1%	21.0%

Table 3

HPLC metabolite analysis of rat blood

	5 min	30 min	60 min	90 min
[^{18}F]**TZ3108**	88.5%	86.5%	78.2%	72.0%
Metabolite 1	3.5%	7.4%	13.7%	13.4%
Metabolite 2	4.3%	3.6%	6.0%	7.5%

Table 4

HPLC metabolite analysis of rat brain

	5 min	30 min	60 min	90 min
[^{18}F]**TZ3108**	96.3%	94.5%	95.1%	95.2%
Metabolite 1	0.01%	0.2%	0.2%	0.1%